STUDY, DESIGN AND FABRICATE A COLD CRUCIBLE SYSTEM

Joseph F. Wenckus, et al

Arthur D. Little, Incorporated

Prepared for:

Air Force Cambridge Research Laboratories

15 May 1974

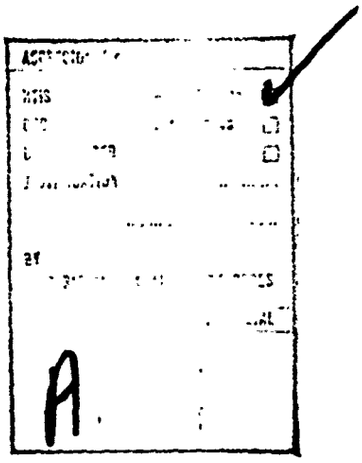

Qualified requestors may obtain additional copies from the Defense Documentation Center. All others should apply to the National Technical Information Service.

AD-786481

SECURITY CLASSIFICATION OF THIS PAGE (When Data Entered)

REPORT DOCUMENTATION PAGE

READ INSTRUCTIONS BEFORE COMPLETING FORM

1. REPORT NUMBER: AFCRL-TR-74-0314	2. GOVT ACCESSION NO.
3. RECIPIENT'S CATALOG NUMBER	
4. TITLE (and Subtitle): STUDY, DESIGN AND FABRICATE A COLD CRUCIBLE SYSTEM	5. TYPE OF REPORT & PERIOD COVERED: Scientific Report No. 1
6. PERFORMING ORG. REPORT NUMBER	
7. AUTHOR(s): Joseph F. Wenckus, Martin L. Cohen, Alfred G. Emslie, Wilson P. Menashi, Peter F. Strong	8. CONTRACT OR GRANT NUMBER(s): F19628-74-C-0097
9. PERFORMING ORGANIZATION NAME AND ADDRESS: Arthur D. Little, Inc. 15 Acorn Park, Cambridge, MA 02140	10. PROGRAM ELEMENT, PROJECT, TASK AREA & WORK UNIT NUMBERS: 61102F, 5620-09-06 681306
11. CONTROLLING OFFICE NAME AND ADDRESS: Air Force Cambridge Research Laboratories (LQ) Hanscom AFB, MA 01730 Contract Monitor: Joseph J. Hutta/LQP	12. REPORT DATE: May 15, 1974
	13. NUMBER OF PAGES: 54
14. MONITORING AGENCY NAME & ADDRESS (if different from Controlling Office)	15. SECURITY CLASS. (of this report): Unclassified
	15a. DECLASSIFICATION/DOWNGRADING SCHEDULE

16. DISTRIBUTION STATEMENT (of this Report)

A - Approved for public release; distribution unlimited.

17. DISTRIBUTION STATEMENT (of the abstract entered in Block 20, if different from Report)

18. SUPPLEMENTARY NOTES

Tech., Other

19. KEY WORDS (Continue on reverse side if necessary and identify by block number)

Cold Crucible System, Semiconductors, Oxides

20. ABSTRACT (Continue on reverse side if necessary and identify by block number)

The objective of this program is to conduct a study, design and fabricate a cold crucible system for the synthesis and Czochralski crystal growth of refractory semiconductors and oxides. During the first 6 months a theoretical analysis of the cold crucible relating the properties of the material to the electrical characteristics of the cold crucible has been essentially completed. The thermal analysis, which includes thermal modeling by means of a computer technique, has also been completed. Ar

DD FORM 1 JAN 73 1473 EDITION OF 1 NOV 65 IS OBSOLETE

Unclassified

SECURITY CLASSIFICATION OF THIS PAGE (When Data Entered)

initial detailed analysis of the RF power control system necessary to provide the desired stability for crystal growth has been completed.

The design of a cold crucible assembly suitable for the growth or refractory oxide crystals has been completed. It is a simple, rugged, modular assembly which will be readily adaptable in the future to a controlled-atmosphere furnace system.

We plan to use a 50 KW (5-7 MHz) RF power generator manufactured by Fritz Heuttinger Elektronik GmbH (Freiburg, Germany) for the performance testing of the cold crucible assembly. This particular system was selected because of its unique circuit design to provide for high stability under widely-varying load conditions. Delivery of this system from Germany is expected shortly.

TECHNICAL SUMMARY

The objective of this program is to conduct a study, design and fabricate a cold crucible system for the synthesis and Czochralski crystal growth of refractory semiconductors and oxides. Specifically, the work to be performed is:

Study by theoretical analysis of the cold crucible to relate the properties of materials to the electrical and thermal characteristics of the cold crucible and define a control system to provide a high degree of stability for crystal growth.

Design a cold crucible assembly complete with control system suitable for oxide crystal growing. Define the criteria necessary for integrating the cold crucible system with a controlled atmosphere (up to 100 atmospheres) crystal growing furnace.

Fabricate a cold crucible assembly complete with control system. Test and evaluate these to explore the operating techniques suitable for crystal growing applications, and demonstrate high temperature operation under oxidizing conditions.

During the past 6 months the following topics were covered:

1. The theoretical analysis of the cold crucible relating the properties of the material to the electrical characteristics of the cold crucible was completed. The thermal analysis, which includes thermal modeling by means of a computer technique, has also been completed. During the course of the program it is anticipated that it may prove necessary to refine the analyses following the operating tests of the cold crucible assembly.

2. A detailed analysis of the RF power control system necessary to provide the desired stability for crystal growth has been completed. It may also be necessary to partially modify the control system following runs carried out in the cold crucible assembly.

3. The design of a cold crucible assembly suitable for the growth of refractory oxide crystals has been completed. Based upon the guidelines established by the theoretical analysis, as well as first-hand knowledge of cold crucible configurations which are currently operating with considerable success in the U.S.S.R., we have designed a simple, rugged, modular assembly which will be readily adaptable in the future to a controlled-atmosphere furnace system.

4. We plan to use a 50 KW (5-7 MHz) RF power generator manufactured by Fritz Huettinger Elektronik GmbH (Freiburg, Germany) for the performance testing of the cold crucible assembly. This particular system was selected because of its unique circuit design which provides for high stability under widely-varying load conditions.

   Delivery of this system from Germany was originally expected by year end 1973; however, it has been seriously delayed due to the world-wide shortage of vendor-supplied electronic components. We have recently been informed that the apparatus will be undergoing testing during the last week of April and hopefully will be air-shipped to the United States by the end of May.

PREFACE

Major advances in the development of cold crucibles, i.e. water-cooled metal crucibles for use with RF induction heating, used for "skull melting" have taken place in the past two years with significant impact on refractory materials technology. For the first time, it is possible to contain stable, uncontaminated melts of even the most refractory materials for which no crucible exists.

Russian scientists at the Lebedev Physical Institute in Moscow have developed skull melting to a point where it has become a reproducible production operation. Oxide melts at temperatures up to 3000°C with weights up to 25 kilograms are being used in the production of a wide variety of strategic materials including unique laser crystals, refractory optical elements and melt-cast ceramics.

The new process involves direct high-frequency induction heating of the material contained in a water-cooled, crucible-like structure. The melt formed is contained by a sintered shell or "skull" of identical composition so that the problems of reaction and contamination, traditionally the most severe problem faced in the containment of refractory melts, have been virtually eliminated. The melt can then be cast or recrystallized using standard methods of crystal growth.

During the past few years, high-pressure crystal growing furnace systems developed in the United States by Arthur D. Little, Inc., have enabled the materials scientist to cope with the problems of high vapor pressure in producing single crystals of new quantum-electronics materials such as Gallium Phosphide. It now appears feasible to combine the cold crucible with its inert ultra-high temperature capabilities with domestic high-pressure technology to provide a materials research and production tools of unprecedented capabilities.

This report details work performed in the first 6 months of the program during which time theoretical studies were completed, design of the cold crucible assembly finished and work initiated on its construction.

TABLE OF CONTENTS

LIST OF ILLUSTRATIONS

LIST OF TABLES

1.0 INTRODUCTION

The principal objective of the proposed program is the design and development of a skull melting system which can be used for the production of high purity single crystal oxides. Typically, most of the cold crucibles in operation today have evolved by empirical trial and error procedures. A theoretical analysis of the cold crucible has been carried out to relate the properties of the material(s) to be melted to the electrical and thermal characteristics of the cold crucible. Based upon this analysis we have established basic guidelines for the design and construction of cold crucible assemblies.

One of the major problems as yet unresolved in the use of the cold crucible for the growth of single crystals is related to the stabilization and precise control of melt temperature. We have analyzed the critical control parameters of the cold crucible and, based upon the unique RF power control techniques which have been developed in the United States, have defined a control system to provide the high degree of stability necessary for crystal growing applications.

A cold crucible assembly complete with control system suitable for oxide crystal growing operation has been designed and is being constructed. Testing and evaluation of the cold crucible assembly and control system will be carried out to explore the operating techniques suitable for crystal growing applications. An oxide such as stabilized zirconia (M.P. 2690°C) will be used to demonstrate very high temperature operation under oxidizing conditions. We will then deliver a cold crucible assembly to the Air Force Cambridge Research Laboratories.

The ultimate goal of this work is the integration of the cold crucible system into a crystal growing furnace chamber capable of operation under controlled atmosphere at pressures up to 100 atmos. It should be realized, however,

that the integration of two sophisticated techniques may lead to the identification of problems which we do not foresee at present. During the course of this program we shall attempt to define the necessary parameters for practical integration.

2.0 TECHNICAL DISCUSSION

2.1 Introduction

During the past 6 months we have:

1. Theoretically analyzed the electrical characteristics of the cold crucible system. The problems involved and the conclusions are presented in Section 2.2 while the derivation is discussed in Appendix A.

2. Theoretically analyzed the thermal characteristics of the cold crucible. The conclusions are presented in Section 2.3 and the derivation shown in Appendix B.

3. Theoretically analyzed the control of the RF power. This is discussed in Section 2.4 and the derivation is presented in Appendix C.

4. Designed and initiated construction on the cold crucible assembly. Refer to Section 2.5 for review of the design criteria.

2.2 Theoretical Analysis of the Electrical Characteristics of the Cold Crucible

The following problems involved in skull melting of refractory materials have been theoretically analyzed:

- The effect of the copper cage on the magnetic field applied to the refractory charge.

- The resistive and inductive effect of the cage on the radio frequency coil.

- The effect of the skin depth of field penetration on the total power input to the charge.

- The spatial distribution of the power input.

- The resistive loading of the RF coil due to power absorbed by the charge.

- The RF magnetic field required to melt metal particles in the charge to achieve startup.

It is found that a properly designed cage has no effect on the field applied to the charge. The cage merely lowers the inductance of the RF coil slightly by excluding the field from the volume occupied by the cage tubing and adds a small resistive loading to the coil.

The power delivered to the molten charge by a given applied RF field is calculated for a disk-shaped charge approximated by an ellipsoid of revolution. This is done for the field penetration skin depth both large and small compared with the smallest semi-axis of the ellipsoid. These two limiting cases converge toward a common maximum value of the power when the skin depth in each case approaches the size of the semi-axis. For an ellipsoid of dimensions 8 cm x 8 cm x 2 cm in a field of 1000 A/m, this maximum power is several kilowatts.

The calculations show that the heating power is strongly concentrated around the equator of the ellipsoid, especially when the skin depth is small compared with the thickness of the ellipsoid. An expression is derived for the resistive loading of the RF coil by the induced currents in the molten charge.

Startup by means of 2 mm diameter metal spheres embedded in the powdered charge is found to be theoretically feasible but requires a starting field perhaps 10 times larger than that needed to maintain the melt.

2.3 Thermal Analysis of the Cold Crucible

During this quarter the thermal analysis of the melt and the powder when heated by the induced RF currents and cooled by the walls of the container was completed. We find that:

- The molten region tends to take the shape of a flattened body of revolution; it acts as a fin, with the source of heat in a ring near the equatorial plane near the surface of the body. Heat travels inwards and is lost by radiation and conduction along the way.

- If a substantial heat loss from the top surface of the melt occurs, the shape of the melt is very sensitive to the amount thus lost.

- There should be a large amount of powder to insulate the melt on its under side, although the exact amount is not critical. This means that the molten zone should be confined to the upper portion of the cooled container.

Thermal models have been developed for typical skull melting systems and the effects of heat sources and sinks upon melt shape have been computer-profiled and are discussed in Appendix B.

2.4 Control of RF Power

Precise control of the RF power is required for successful crystal growth. There is a basic tendency toward instability when induction

heating is used directly to melt semiconductors and refractory oxides. Therefore, a radio frequency current control system will be used to maintain a constant RF magnetic field.

The balance between heat loss and heat generation processes result in a stable system in this case. Past experience shows that the control system response time can be as fast as one second. The thermal time constant of the charge will be longer than this, with the result that temperature fluctuations due to external disturbances will be small.

We expect to obtain fields as strong as 10^4 amperes per meter if necessary, which will permit utilization of the full output of the RF power source.

2.5 Design and Construction of the Cold Crucible Assembly

Based upon the electrical and thermal analyses which have been carried out, we have completed the design of a cold crucible assembly which is shown in Figure 1. The copper structure has been designed for high pressure operation and integration with the ADL crystal growing furnaces presently in use at the Air Force Cambridge Research Laboratories. Construction of the cold crucible assembly has been initiated.

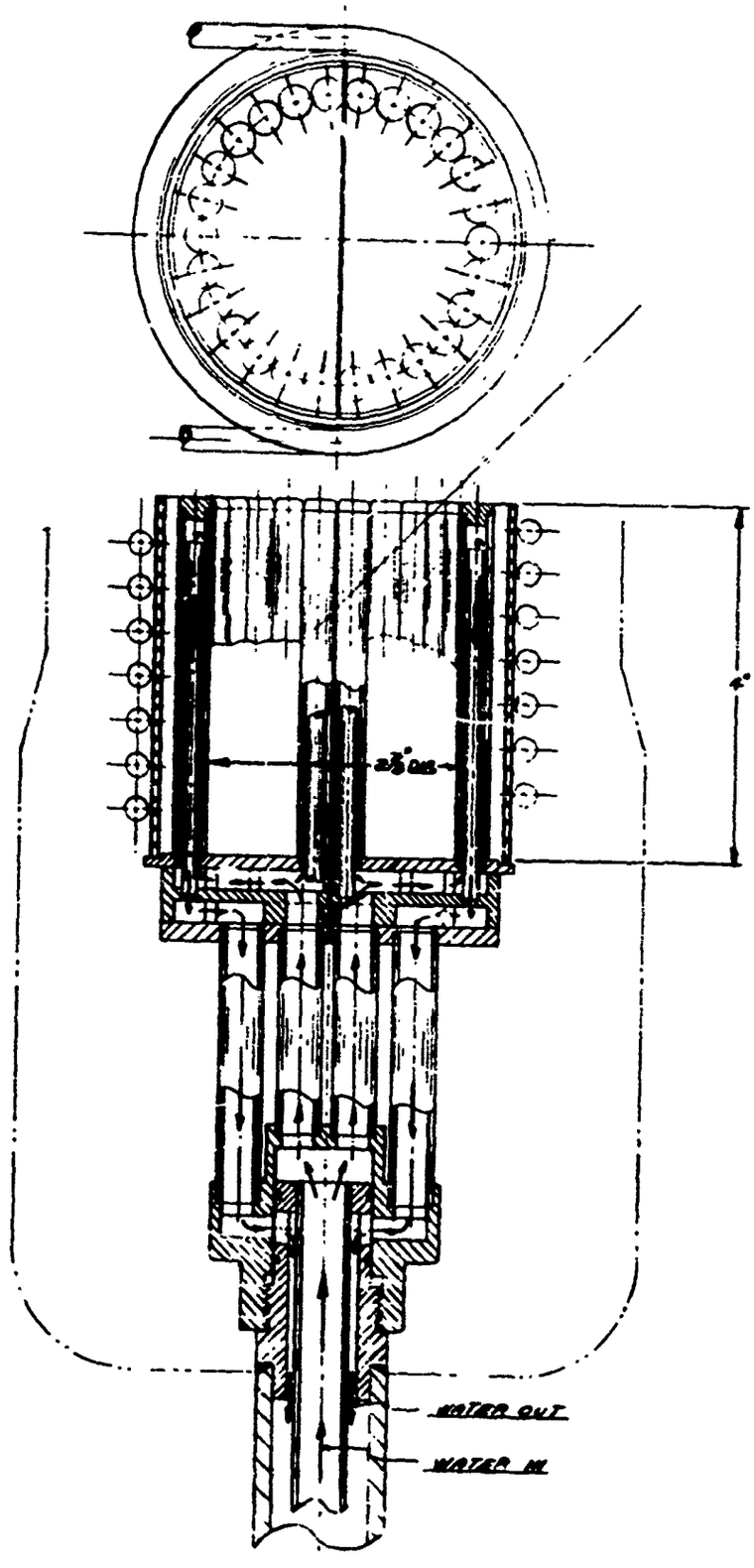

FIGURE 1 ADL COLD CRUCIBLE ASSEMBLY

3.0 FUTURE WORK

- The construction of the cold crucible assembly will be completed.
- Upon receipt and installation of the high frequency RF power supply (Heuttinger Elektronik), testing and evaluation of the cold crucible assembly will be initiated.
- Performance characteristics of the cold crucible assembly will be determined and experiments involving the melting of refractory oxides under oxidizing conditions will proceed.
- During the course of these experiments, it is anticipated that the criteria for integration of the cold crucible assembly within a controlled atmosphere furnace will be developed.
- The cold crucible assembly (less control system) will be delivered to the Air Force Cambridge Research Laboratories.

APPENDIX A

THEORETICAL ANALYSIS OF THE ELECTRICAL CHARACTERISTICS OF SKULL MELTING

A.1 Effect of the Cage

We assume that the cage consists of vertical copper tubes parallel to the axis of the coil as shown in cross section in Figure A.1. The effect of the bottom of the cage is small and will be neglected here.

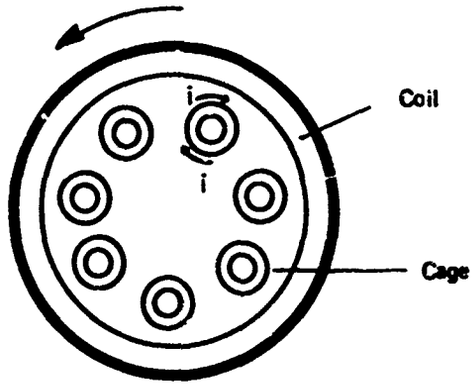

CROSS SECTION OF SKULL MELTING CAGE

FIGURE A.1

If the coil has n turns and a length ℓ and carries an alternating current, I, the rms current per unit length is

$$i = \frac{nI}{\ell} \text{ (A/m)} \qquad (1)$$

and the axial magnetic field is

$$H_0 = \frac{nI}{\ell} \text{ (A/m)} \qquad (2)$$

At frequencies in the range 1-10 MHz, the skin depth of penetration of the field into the copper tubes of the cage is only about 2×10^{-5}m. The copper therefore essentially excludes the field and acts like an almost perfect diamagnetic material. Under these conditions each tube has a circulating current per unit length equal to -i (A/m).

The energy stored in the field is

$$E = \frac{\mu_0}{2} H_0^2 \, \ell \, (A_{coil} - A_{cage}) \quad \text{(Joule)} \tag{3}$$

where the A's are the cross-sectional areas of coil and cage and where $\mu_0 = 4\pi \times 10^{-7}$ Henry/m and is the permeability of free space. From Equation 2 the expression becomes

$$E = \frac{\mu_0}{2} \frac{n^2 I^2 \, (A_{coil} - A_{cage})}{\ell} \tag{4}$$

The energy can also be expressed in terms of the net self-inductance, L, of the assembly by the relation

$$E = \frac{1}{2} L I^2 \tag{5}$$

On equating 4 and 5, we obtain for the inductance

$$L = n^2 \mu_0 \frac{(A_{coil} - A_{cage})}{\ell} \quad \text{(Henry)} \tag{6}$$

The cage, therefore, reduces the inductance of the coil by a factor $(A_{coil} - A_{cage})/A_{coil}$.

The cage also adds some series resistance to the coil. The circumferential current, i, in a tube of the cage is distribution in depth, x, into the copper according to the approximate formula

$$J = \frac{i}{\delta} e^{-x/\delta} \tag{7}$$

where J is the current density (A/m), and δ is the skin depth, given by the relation

$$\delta = \sqrt{\frac{1}{\pi \mu_0 f \sigma}} \tag{8}$$

Here f is the frequency (Hz) and σ is the conductivity of copper (mhos/m).

The power dissipated per unit area of tube surface is then

$$W'' = \int_0^\infty \frac{J^2}{\sigma} dx = \frac{i^2}{2\sigma\delta} \quad (W/m^2) \tag{9}$$

The total power for N tubes of height, h, and diameter, D, is

$$W = \frac{N \pi D h i^2}{2\sigma\delta} = \frac{n^2 N\pi Dh I^2}{2\sigma \ell^2 \delta} \tag{10}$$

and the effective series resistance introduced into the coil is therefore

$$R = \frac{n^2 N\pi Dh}{2\sigma \ell^2 \delta} \tag{11}$$

We have assumed that $h<\ell$. If the tubes are longer than the coil, h, in Equation 11, is replaced by ℓ.

A.2 Heat Input to the Charge

We assume for mathematical convenience that the charge has the shape of an oblate spheroid, which is a good approximation to the actual

disk-like shape. The equation of the surface is

$$\frac{r^2}{a^2} + \frac{z^2}{c^2} = 1 \qquad (12)$$

where a and c are the semi-axes of the spheroid, and z and r are vertical and horizontal cylindrical coordinates.

The distribution of induced current in the spheroid depends strongly on the skin depth, δ, in the molten material. The two limiting cases, $\delta >> c$ and $\delta << c$, are mathematically tractable, while the intermediate case, $\delta \sim c$, is too difficult for analytical treatment. The limiting cases, however, serve to bracket the intermediate case and give considerable insight into the general problem.

A.2.1 Large Skin Depth

When $\delta >> c$, the uniform magnetic field, H_0, produced by the coil, penetrates the charge with little distortion. Under these conditions the induced circumferential electric field, E_θ, is given by the simple circuital emf equation.

$$2\pi r\, E_\theta = -\frac{\partial}{\partial t}(\pi r^2 B) = -\pi r^2 \mu_0\, j\omega\, H_0 \qquad (13)$$

where $\pi r^2 B$ is the instantaneous magnetic flux through a circle of radius, r, and ω is the angular frequency.

The associated current density is

$$J_\theta = \sigma E_\theta = -\frac{j}{2}\sigma\mu_0\, \omega\, r\, H_0 \qquad (14)$$

The rate of heat generation per unit volume at the radius, r, is

$$W''' = \frac{1}{\sigma} |J_\theta|^2 = \frac{1}{4} \sigma \mu_0^2 \omega^2 r^2 H_0^2 \qquad (15)$$

The power per unit area projected on the (x,y) plane is, from Equation 12,

$$W'' = 2z\, W''' = \frac{1}{2} \sigma \mu_0^2 \omega^2 H_0^2 c\, r^2 \sqrt{1 - \frac{r^2}{a^2}} \qquad (16)$$

It is to be noted that W'' is zero at both r = 0 and r = a and is maximum at $r = a\sqrt{2/3} = 0.816a$.

The total heating rate for the whole ellipsoid is

$$W = \int_0^a W'' \, 2\pi r dr = \frac{2\pi}{15} \sigma \mu_0^2 \omega^2 a^4 c H_0^2 \qquad (17)$$

From Equation 8, this can also be written, in terms of δ instead of α, as

$$W = \frac{4\pi}{15} \frac{\mu_0 \omega a^4 c H_0^2}{\delta^2} \qquad (18)$$

As a numerical example we take the following values:

$$\mu_0 = 4\pi \times 10^{-7} \quad H/m$$

$$f = 10 \times 10^6 \quad MHz$$

$$a = 0.04m$$

$$c = 0.01m$$

$$\delta = 2c = 0.02m$$

$$H_0 = 1000 \quad A/m$$

Then W = 4000 watt.

The value chosen for δ corresponds to σ = 63 mho/m and is probably near the limit of validity of the theory. The value of H_0 corresponds to that for a 5-turn coil of length 10cm carrying a current of 20 amperes.

A.2.2 Small Skin Depth

The case, $\delta << c$, may not occur in practice for the range of conductivities likely to be formed for molten refractory materials, without the use of frequencies well in excess of 10 MHz. However, it is still of value to determine the power distribution in the charge for this limiting case.

Like the cage tubing, the spheroid acts like a nearly perfect diamagnetic body when $\delta << c$. The current distribution on the surface of the spheroid is such that the external magnetic field is the same as that produced by a uniformly magnetized body of the same shape. The intensity of magnetization, m, (dipole moment per unit volume) is related to the applied field, H_0, of the coil by the formula

$$m = \frac{H_0}{1-N} \tag{19}$$

where N is the demagnetization factor, which depends on the ellipsoid shape. For a sphere N = 1/3. For an oblate spheroid with semi-axes, a, a, c, the factor is given by[8]

$$N = \left(\frac{1 + k^2}{k^2}\right) \left(1 - \frac{1}{k} \tan^{-1} k\right) \tag{20}$$

where

$$k = \sqrt{\frac{a^2}{c^2} - 1} \qquad (21)$$

Table A.1 shows how N varies with c/a.

TABLE A.1

DEMAGNETIZATION FACTOR N

$\frac{c}{a}$	N
0.0	1.000
0.2	0.750
0.4	0.588
0.6	0.478
0.8	0.396
1.0	0.333

For the shape of interest here, where c/a - 1/4, N = 0.7037. For this value the intensity of magnetization is from Equation 19

$$m = - 3.375\ H_0 \qquad (22)$$

Knowing m, and therefore the effective distribution of magnetic charge density over the surface of the spheroid, one can calculate the magnetic field distribution and from it the equivalent surface current distribution.

In Figure A.2 we consider the ellipsoid as a perfect diamagnetic body with permeability $\mu = 0$. Then the magnetic induction, B_i,

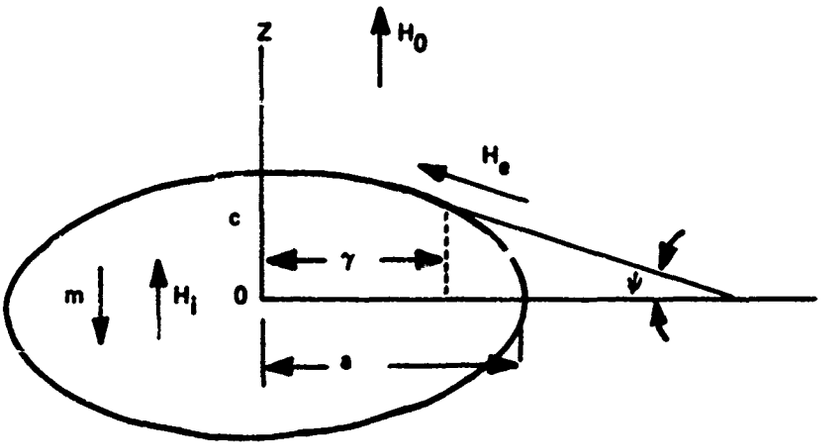

THE ELLIPSOID AS A PERFECT DIAMAGNETIC BODY

FIGURE A.2

within the ellipsoid is given by

$$B_i = \mu H_i = 0 \tag{23}$$

Also,

$$B_i = H_i + m \tag{24}$$

The directions of H_i and m are shown in Figure A.2.

We now apply the boundary condition that the tangential component of H is continuous. Now the field, H_e, just outside the ellipsoid is known to be tangential, as indicated in Figure A.2. Therefore, just below the surface, $H_i = H_e$, as shown in the vector diagram in Figure A.3 where the vector sum of H_e and H_n equals the internal field, H_i.

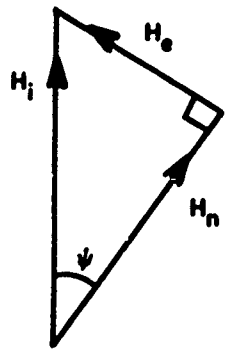

MAGNETIC FIELD VECTORS

FIGURE A.3

From the diagram we obtain the result

$$H_e = H_i \sin \psi = - m \sin \psi \qquad (25)$$

where the angle, ψ, is defined in Figure A.2.

On substitution for m from Equation 19 we find that

$$H_e = \frac{H_0 \sin \psi}{1 - N} \qquad (26)$$

The surface current, (A/m), is therefore

$$I = \frac{H_0}{1 - N} \frac{c \cos \phi}{\sqrt{a^2 \sin^2 \phi + c^2 \cos^2 \phi}} \qquad (27)$$

The total power is

$$W = \int R_s \, I^2 \, 2\pi \, r \, ds \tag{28}$$

where R_s is the surface resistance, (ohm/□), given by Equation 4 as

$$R_s = \frac{1}{2\sigma\delta} \tag{29}$$

and ds is an element of arc of the ellipsoid given by

$$ds = \sqrt{a^2 \sin^2 \phi + c^2 \cos^2 \phi} \cdot d\phi \tag{30}$$

From Equations 27-30 we obtain for the power

$$W = \frac{\pi a c^2 H_0^2}{\sigma\delta(1 - N)^2} \int_{-\frac{\pi}{2}}^{\pi/2} \frac{\cos^3 \phi \, d\phi}{\sqrt{a^2 \cos^2 \phi + c^2 \sin^2 \phi}}$$

$$= \frac{a^2 H_0^2}{\sigma\delta} \cdot \frac{\pi c \, F(\frac{a}{c})}{(1 - N)^2} \tag{31}$$

where

$$F(x) = \frac{(2x^2 - 1)}{(x^2 - 1)^{3/2}} \log_e (\sqrt{x^2 - 1} + x) - \frac{x}{x^2 - 1} \tag{32}$$

Table A.2 shows how the second factor in Equation 31 depends on a/c. It can be seen that the power is quite constant for c/a between 0.1 and 1.0 (for fixed a). For very flat ellipsoids the power increases slowly.

TABLE A.2

GEOMETRICAL FACTOR IN EQUATION 31

$\frac{c}{a}$	$\frac{\pi c F \frac{a}{c}}{a(1 - N)^2}$
0.0001	24.020
0.001	18.101
0.01	12.534
0.1	8.190
0.2	7.510
0.25	7.465
0.4	7.564
0.6	8.121
0.8	8.744
1.0	9.425

The radial distribution of the power is also of interest. From Equation 28 we find, on counting the power on both top and bottom of the ellipsoid, that

$$\frac{dW}{dr} = \frac{4\pi R_s H_o^2 C^2}{(1 - N)^2} \cdot G \frac{r}{a} \tag{33}$$

where

$$G\left(\frac{r}{a}\right) = \frac{\left(\frac{r}{a}\right)^3}{\sqrt{\left[1 - \left(1 - \frac{c^2}{a^2}\right)\frac{r^2}{a}\right]\left[1 - \left(\frac{r^2}{a}\right)\right]}} \tag{34}$$

Table A.3 shows how G varies with r/a for the case, c/a = 1/4. The last column in the table gives the fraction of the power within a radius, r. It is seen that the power is strongly concentrated at the equator of the ellipsoid.

TABLE A.3

RADIAL DISTRIBUTION OF POWER FOR c/a = 1/4

$\frac{r}{a}$	$G(\frac{r}{a})$	$\frac{W(r)}{W(a)}$
0.0	.0000	.0000
0.1	.0010	
0.2	.0083	.0001
0.3	.0296	
0.4	.0757	.0021
0.5	.1650	
0.6	.3317	.0121
0.7	.6532	
0.8	1.3492	.0549
0.9	3.4094	
1.0	00	1.0000

For c/a = 1/4 the total power, from Equation 31 and Table A.2, is

$$W = 7.47 \frac{H_0^2 a^2}{\sigma\delta} \qquad (35)$$

We expect that this expression will remain approximately valid for $\delta = c/2 = 0.005$m. At f = 10 MHz, this corresponds to $\sigma = 1000$ mho/m. For a = 0.04m and $H_0 = 1000$ A/m, as before, we find from Equation 35 that W = 2400 watt which is to be compared with the value of 4000 watt calculated on the $\delta >> c$ assumption for $\delta = 0.02$m.

On substituting for σ from Equation 8 we find that Equation 35 takes the form

$$W = 3.73\ \mu_0\ \omega\ a^2\ H_0^2\ \delta \qquad (36)$$

which shows that W tends to zero for very small δ. The limiting expressions, Equations 36 and 18, therefore show that, as δ varies from small to large values, due to variation of the conductivity, W passes through a maximum which, for the numerical values chosen above, probably lies between 2000 and 4000 watts and occurs for $\delta = c = 0.01$m.

A.3 Coil Resistance Due to Load

On substituting for H_0 from Equation 2 into Equation 36, we can express W in terms of the current I in the coil by the formula

$$W = \frac{4.78\ \mu_0\ \omega\ a^2\ \delta\ n^2\ I^2}{\ell^2} \qquad (37)$$

The load therefore acts like a resistance

$$R_L = \frac{4.78\ \mu_0\ \omega\ a^2\ \delta\ n^2}{\ell^2} \quad (\delta << c) \qquad (38)$$

Likewise, from Equation 18 we obtain

$$R_L = \frac{4\pi}{15} \frac{\mu_0\ \omega\ a^4\ c\ n^2}{\ell^2 \delta^2} \quad (\delta >> c) \qquad (39)$$

A.4 Startup

In order to start the inductive heating one must usually add some high-conductivity material such as particles of the same metal as is present in the composition of the charge itself. We consider a metal sphere of radius a and conductivity σ. In the high frequency field, H_0, the sphere acts as a diamagnetic body with a demagnetization factor N = 1/3 (see Table A.1). From Equation 19 the effective

intensity of the magnetization of the sphere is

$$m = -\frac{3}{2} H_0 \tag{40}$$

The total magnetic moment of the sphere is

$$M = \frac{4}{3}\pi a^3 m = -2\pi a^3 H_0 \tag{41}$$

For the special case of the sphere, unlike that of a spheroid, the moment, M, acts as though it were located at the center of the sphere. The tangential magnetic field at the surface of the sphere, due to M, is

$$(H_0)_{\text{dipole}} = \frac{M \sin\theta}{4\pi a^3} = -\frac{1}{2} H_0 \sin\theta \tag{42}$$

where θ is the polar angle.

Since the applied field, H_0, gives a tangential component, $-H_0 \sin\theta$, at the surface of the sphere, the total tangential field is

$$H_0 = -\frac{3}{2} H_0 \sin\theta \tag{43}$$

The circumferential current per unit length on the sphere is therefore

$$i_\phi = -\frac{3}{2} H_0 \sin\theta \tag{44}$$

since it equals the discontinuity in H_0 at the surface of the sphere.

The surface resistance R_s is given by Equation 32. On multiplying this by i_ϕ^2 and integrating over the area of the sphere, we obtain for the power input to the sphere

$$W = \int_0^{\pi} \left(\frac{1}{2\sigma\delta}\right)\left(\frac{9}{4} H_0^2 \sin^2\theta\right) 2\pi a^2 \sin\theta d\theta = \frac{3 H_0^2 a^2}{\sigma\delta} \qquad (45)$$

It is of interest to consider that this power is balanced by blackbody radiation from the surface of the sphere at absolute temperature, T, with the surroundings at temperature, T. Then

$$4\pi a^2 \sigma_0 (T^4 - T_0^4) = \frac{3\pi H_0^2}{\sigma\delta} \qquad (46)$$

or

$$\sigma_0 (T^4 - T_0^4) = \frac{3 H_0^2}{4\sigma\delta} \qquad (47)$$

where $\sigma_0 = 5.672 \times 10^{-8}$ W m^{-2} deg^{-4} is the Stefan-Boltzmann constant. Equation 47 shows that the equilibrium temperature is independent of the radius of the sphere. For the case of a field, H_0 = 1000 A/m, as before, and with $\sigma = 5.0 \times 10^{-5}$m, $\sigma_0(T^4 - T_0^4)$ = 1500 W/m , and T - 431 K. The metal sphere would therefore not melt for the field assumed. However, for a ten times greater field of 10,000 A/m, which is not unreasonable, we get

$$\sigma_0 (T^4 - T_0^4) = 150{,}000 \text{ W/m}^2$$

and

$$T = 1276 \text{ K}$$

which will melt certain metals.

A more appropriate assumption for skull melting is that the metal sphere is embedded in a powder of thermal conductivity K. Then the equilibrium temperature is given by

$$T - T_0 = \frac{W}{4\pi Ka} \tag{48}$$

For K = 0.1 watt/(m deg K), a = 1 x 10^{-3}m, H_0 = 10,000 A/m, and the other constants the same as before, we find that W = 1.88 watt and T = 1600°K. The particle would therefore raise the temperature of the surrounding powder to a value where inductive heating of the powder would occur.

APPENDIX B

THEORY OF THE THERMAL CHARACTERISTICS OF SKULL MELTING

It has been established already that the currents produced in an oblate spheroid by an induction heater are largely concentrated around an equatorial ring which is located near the surface. While the current density as a function of position has been derived rigorously only for the oblate spheroid, the results for this case give us much insight and enable us to anticipate what will probably happen in the case of a more complicated body of revolution whose radius is large compared with its thickness in the axial direction and which is an electrical conductor.

Qualitatively speaking, we may say that the currents in the body will establish themselves in such a way as to exclude most of the field impressed by the induction heater coil. The value of B produced by a ring of current depends mainly on the current, and not so much on the radius of the ring (in a solenoid, the value of H is independent of the radius of the coil), whereas the total flux produced is the product of the area of the ring and the average value of B within the ring. Therefore, in the case of a conductor which is a flattened convex body of revolution, one may expect that the induced current will be largely concentrated in a ring of the largest possible radius which is contained in the body. It is probably best to leave this kind of qualitative argument in its present rather vague state, and simply to conclude that it is of interest to study the shape of the isotherm at the melting temperature in a region filled with a powder of low thermal conductivity, which contains a ring source and which is fairly closely contained by a vessel (represented by an isotherm at 300°K) maintained at room temperature. We will also suppose that near the top of the vessel a rather large amount of heat is lost in order to simulate the conditions that must obtain when the crystal is being pulled slowly from the melt through an aperture above.

One way to approach the problem is to take the shape of the 300K isotherm from the drawing of the tubes containing the coolant and to solve rigorously the boundary value problem thus defined. However, the physical parameters involved (for example the thermal conductivity of the powder, which will depend upon its packing and any sintering that may take place) are very poorly known, so it is not justified to use such rigorous procedure. Instead we may employ a simpler technique and obtain at least a preliminary understanding of the effects on the molten zone that will be produced by variations in the main features of the system. Without great difficulty some important results can thus be obtained which will serve as guide posts in the experimental program.

In doing the simplified problem we are at liberty to place sources and sinks of various strengths at such locations as we choose, provided that these locations are outside the region of interest, which we will take to be bounded by the 300K isotherm. Of course the ring source, which is used to model the induction heating, must be within the melt. We make use of external sources and sinks to model the loss of heat from the top and to control the shape of the 300K isotherm.

It appears that the 300K isotherm must pass close to the ring source in the melt in order to give the isotherm at the melting point its expected flat shape. Also, we want the 300K isotherm to be close to the melt at the top (to model the loss of heat through the aperture used to extract the crystal) and otherwise to resemble, at least roughly, the shape of the cup formed by the tubes containing the coolant.

In Figure B.1 we show what we have taken to be the "standard" arrangement for the 300K and 2318K isotherms (the melting point of alumina is 2318K). The positions of the sources and three sinks are shown and the drawing is to scale, as indicated. The arrangement pictured in Figure B.1 was obtained after a number of mathematical experiments; one lesson that was learned very early is that the 300K sink on the axis has a drastic effect on the shape of the

melt, and that the lower surface of the melt needs to be well insulated. The melt is, in effect, acting as a fin, with the heat traveling towards the center and being lost along the way. The insulation along the under side, which serves to keep the heat loss to a minimum, can be obtained by making sure that the molten zone is in the top part of the cooled container, so that a thick blanket of powder is left unmelted beneath the 2318K isotherm.

We will now illustrate the sensitivity of the shape of the molten region to changes in some of the system parameters by means of figures which show the two standard isotherms and two slightly distorted isotherms. The distorted isotherms are obtained by solving the problem with some changes in the boundary conditions.

In Figure B.2 we show two pairs of isotherms to demonstrate the sensitivity of the shape of the melt to a variation in the position of the upper part of the 300K isotherm from the standard position. The lower part of the 300K isotherm has been held nearly in place. It is clearly seen that the top surface of the melt moves further than the 300K isotherm, while even the bottom part suffers a significant displacement. It is of interest to note that the changes seen are due mainly to a change of 50 watts in the strength of the sink on the axis (from 300W to 250W).

In Figure B.3 we show two pairs of closely spaced isotherms. The lower part of the 300K isotherm has been caused to move about 3mm below its standard position (on the axis), but the corresponding variation in the position of the 2318K isotherm is only about 1mm at the bottom and nearly nothing at the top of the melt. Thus it is seen that the shape of the molten zone is not very sensitive to variations in the geometry of the bottom of the cup, provided that the blanket of insulation is present.

We also determined the sensitivity of the shape of the molten zone to a change in the input power (supplied by the induction heater) by raising the strength of the ring source from 3150 W to 3300W, while the shape of the 300K isotherm

was kept essentially the same as the standard. The result is shown in Figure B.4, which indicates that the shape of the melt is only slightly affected by the change in power input. This is probably due to the fact that the distance between the side of the molten zone and the cold container is very small, so a minute change in this dimension is all that is needed to cause most of the added power to flow directly into the container walls near the plane $z = 0$.

Under certain circumstances it might be desirable to let the molten mass cool slowly, of its own accord, without penetrating the layer of powder that lies over the melt. In such a case one might obtain a symmetrical melt, as shown in Figure B.5.

So far, we have discussed only the case of molten alumina. Another material of interest is zirconia, whose melting point is 2988K. In Figure B.6 we show a set of sources and sinks and the corresponding isotherms at 2988K and 300K. Because of its higher temperature the upper surface of the pool of molten zirconia may be expected to lose much more heat by radiation than is the case with alumina. To allow for this, the strength of the point sink has been set at 800W, and the strengths of the other sources and sinks adjusted in an attempt to produce a suitable configuration of the 2988K and 300K isotherms. While the amount of mathematical experimentation with the model of the higher melting point material has been very limited, we expect that it would be necessary to separate the ring source slightly further from the main ring sink in order to produce a 2988K isotherm that is similar in appearance to the 2318K isotherm of Figure B.1. From an operational point of view, this means that the frequency of the induction locater must be set so as to obtain a large skin depth in the melt.

We expect that the sensitivity of the shape of the zirconia melt to changes in the external configuration will be qualitatively the same as in the case of the alumina melt already discussed.

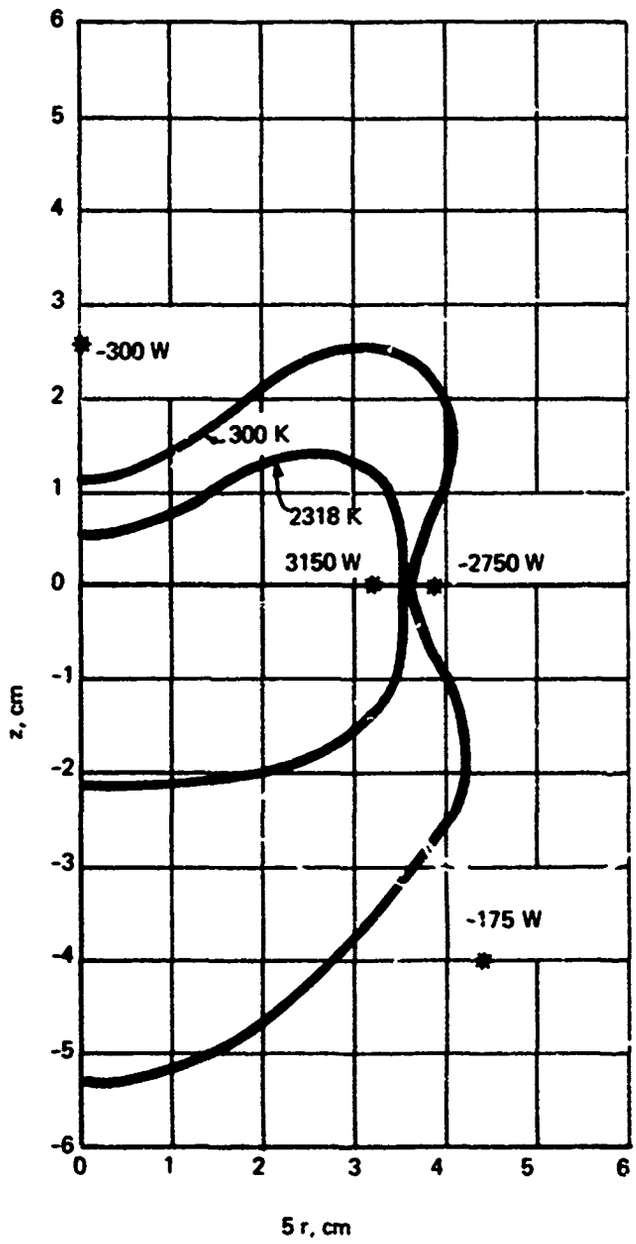

FIGURE B.1 ISOTHERMAL PROJECTION

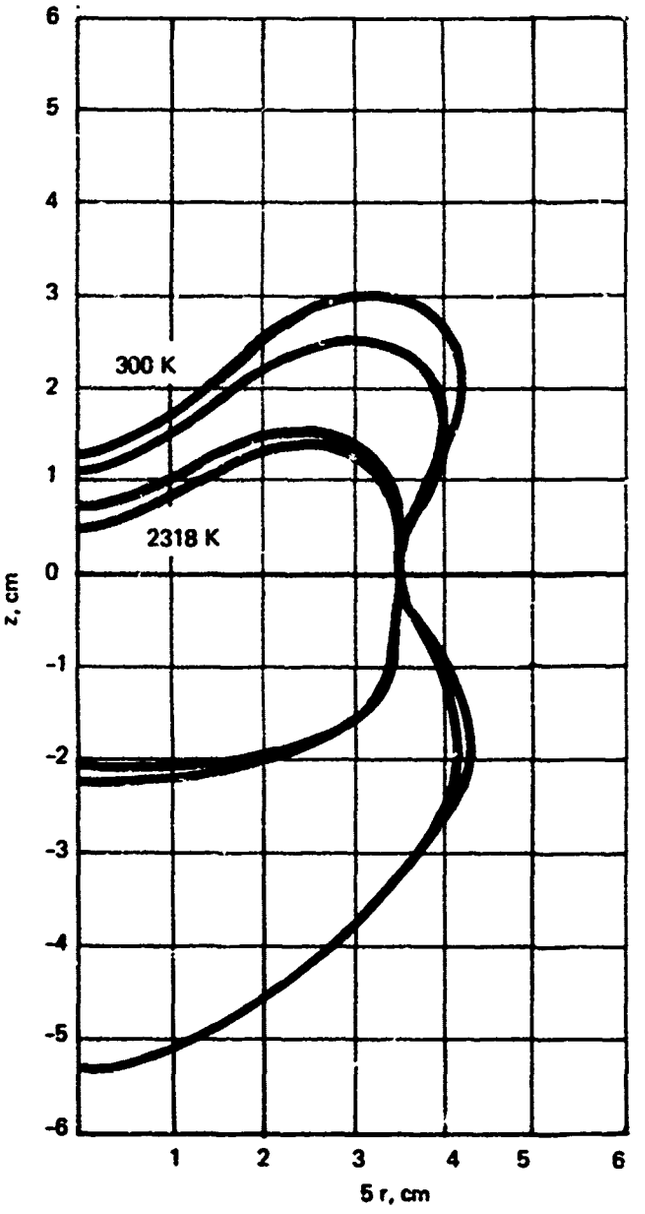

FIGURE B.2 ISOTHERMAL PROJECTION

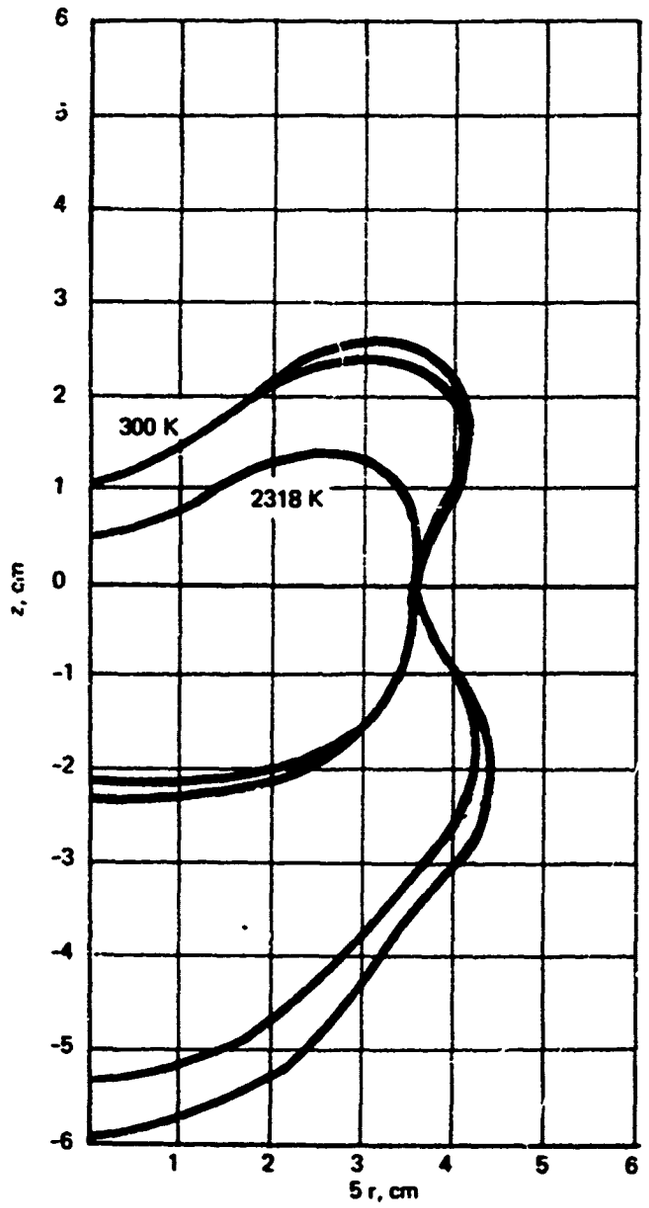

FIGURE B.3 ISOTHERMAL PROJECTION

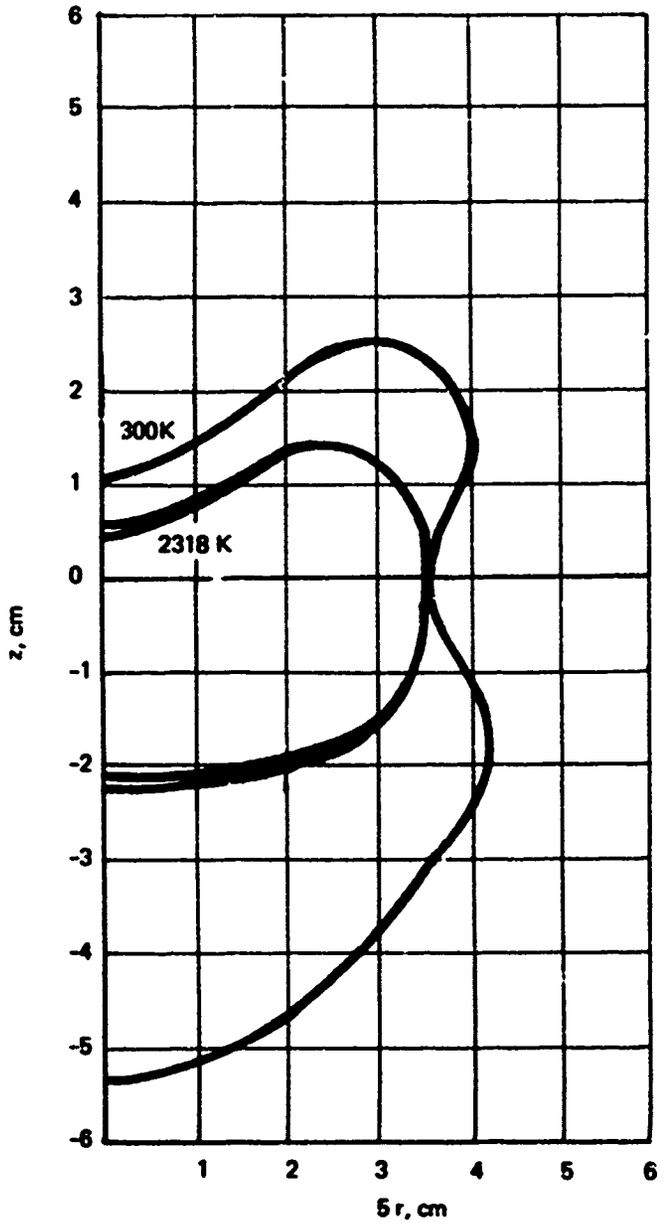

FIGURE B.4 ISOTHERMAL PROJECTION

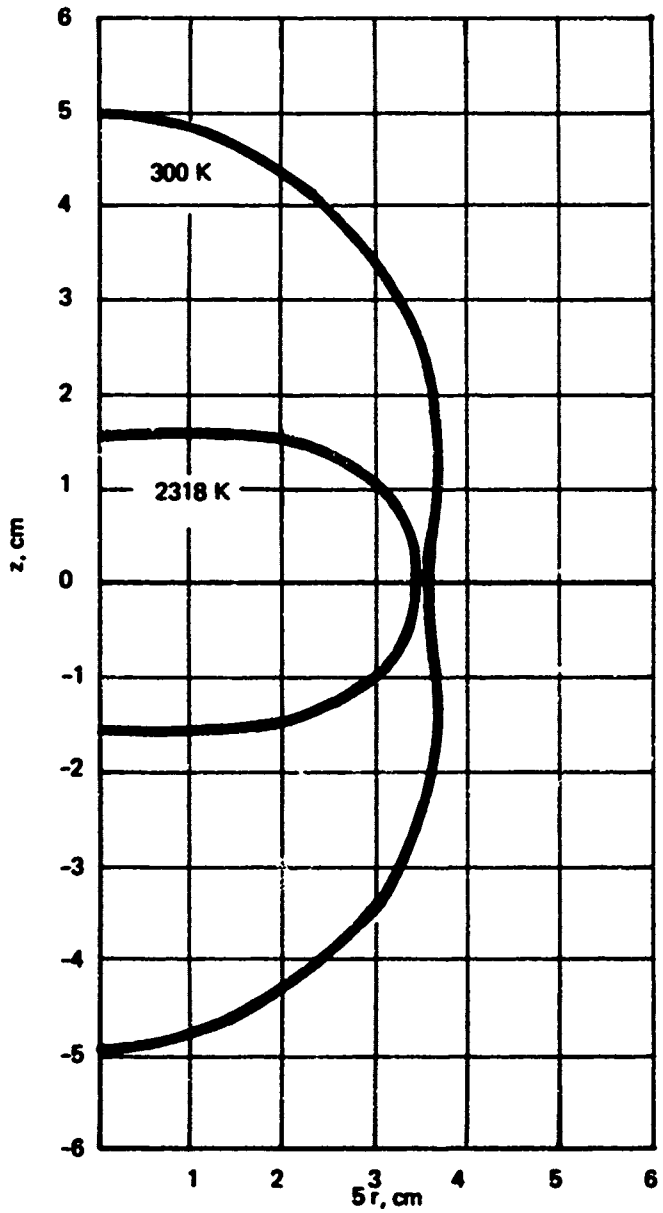

FIGURE B.5 ISOTHERMAL PROJECTION

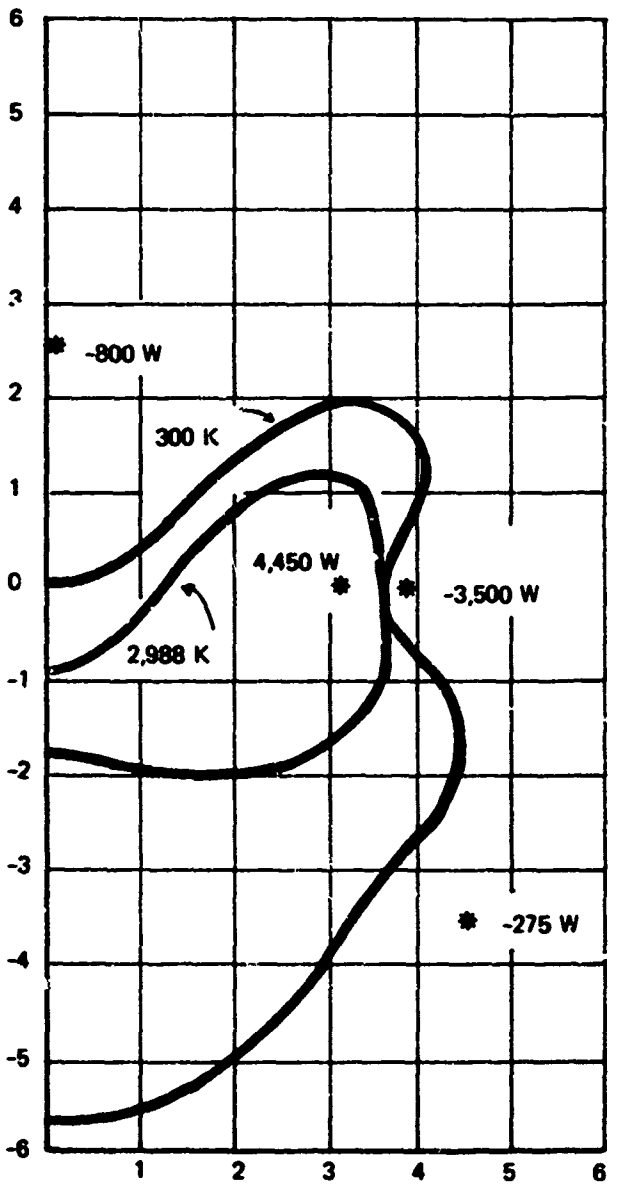

FIGURE B.6 ISOTHERMAL PROJECTION

APPENDIX C

TEMPERATURE DISTRIBUTION DUE TO A RING SOURCE

In this section we derive the formula for the temperature (in steady state) at a point in an infinite medium which contains a source of heat in the form of a ring. We assume the thermal conductivity of the medium to have the fixed value K (watts cm^{-1} deg C^{-1}), so the temperature must satisfy Laplace's equation

$$\nabla^2 T = 0$$

and furthermore we require that the temperature be zero at infinity.

In accordance with these assumptions we find the temperature, dT, at a field point, P, whose coordinates are (x, y, z) produced by a point source of strength dQ watts located at P' with coordinates (x', y', z') to be

$$dT = \frac{dQ}{4\pi K s} \tag{1}$$

where

$$s = \sqrt{(x - x')^2 + (y - y')^2 + (z - z')^2} \tag{2}$$

By adding up the contributions due to many such sources we can, at least in principle, find the temperature due to any distribution of heat sources.

In Figure C.1 we show a ring source of radius, a, located in the z-plane and a field point at an arbitrary point. It is evident from the diagram that

$$\begin{aligned} x' &= a \cos \theta \\ y' &= a \sin \theta \\ z' &= 0 \end{aligned} \tag{3}$$

Now suppose the source to dissipate Q' watts cm^{-1} uniformly along its circumference. Then

$$dQ = Q' \, a d\theta \tag{4}$$

since $ad\theta$ is the element of arc. Therefore we find from the above equation

$$dT = \frac{Q' \, a \, d\theta}{4\pi K\sqrt{(x - a\cos\theta)^2 + (y - a\sin\theta)^2 + z^2}} \tag{5}$$

or, by integration of Equation 5 around the loop,

$$T = \frac{Q'a}{4\pi K} \int_0^{2\pi} \frac{d\theta}{\sqrt{(x - a\cos\theta)^2 + (y - a\sin\theta)^2 + z^2}} \tag{6}$$

On account of the symmetry of the problem we can replace x in Equation 6 by r and replace y by 0. Thus

$$T = \frac{Q'a}{4\pi K} \int_0^{2\pi} \frac{d\theta}{\sqrt{r^2 + a^2 + z^2 - 2ar\cos\theta}} \tag{7}$$

The integral in the right-hand side of Equation 7 is not "elementary", but can be evaluated simply in terms of the well-known complete elliptic integral, $\underline{K}(m)$, which is defined by the formula

$$\underline{K}(m) = \int_0^{\pi/2} \frac{d\phi}{\sqrt{1 - m\sin^2\phi}} \tag{8}$$

First make the substitution

$$\theta = 2\phi + \pi$$

in Equation 7 to obtain

$$T = \frac{Q'a}{2\pi K} \int_{-\pi/2}^{\pi/2} \frac{d\phi}{\sqrt{(a + r)^2 + z^2 - 4ar\sin^2\phi}} \tag{9}$$

Next remove the factor $(a + r)^2 + z^2$ from the expression whose square root is indicated and note, since $\sin^2\phi$ is even, that the range of integration can be reduced by setting the lower limit to zero if a factor of two is

placed in front of the integral. Thus we find

$$T = \frac{Q'a}{\pi K\sqrt{(a + r)^2 + z^2}} \int_0^{\pi/2} \frac{d\phi}{\sqrt{1 - \frac{4ar}{(a + r)^2 + z^2} \sin^2 \phi}} \tag{10}$$

Whence, by the definition of Equation 8, it is clear that

$$T = \frac{Q'a}{\pi K\sqrt{(a + r)^2 + z^2}} \underline{\overline{K}}\left[\frac{4ar}{(a + r)^2 + z^2}\right] \tag{11}$$

The function $\underline{\overline{K}}(m)$ is easily computed by means of the approximations given by Hastings.* Finally we let Q be the total heat dissipated by the ring so

$$Q' = Q/2\pi a$$

and

$$T = \frac{Q}{2\pi^2 K\sqrt{(a + r)^2 + z^2}} \underline{\overline{K}}\left[\frac{4ar}{(a + r)^2 + z^2}\right] \tag{12}$$

If the ring is located at a height, h, instead of at the plane, z = 0, the quantity, z, in Equation 12 must be replaced by the quantity, z - h. Note that $\underline{\overline{K}}(0) = \pi/2$, so a ring source of radius, a = 0, produces a temperature field

$$T = \frac{Q}{4\pi K\sqrt{r^2 + z^2}} \tag{13}$$

This is obviously the field produced by a point source, as it jolly well ought to be.

---

*C. Hastings, Jr.: Approximations for Digital Computers, Princeton University Press, Princeton, New Jersey.

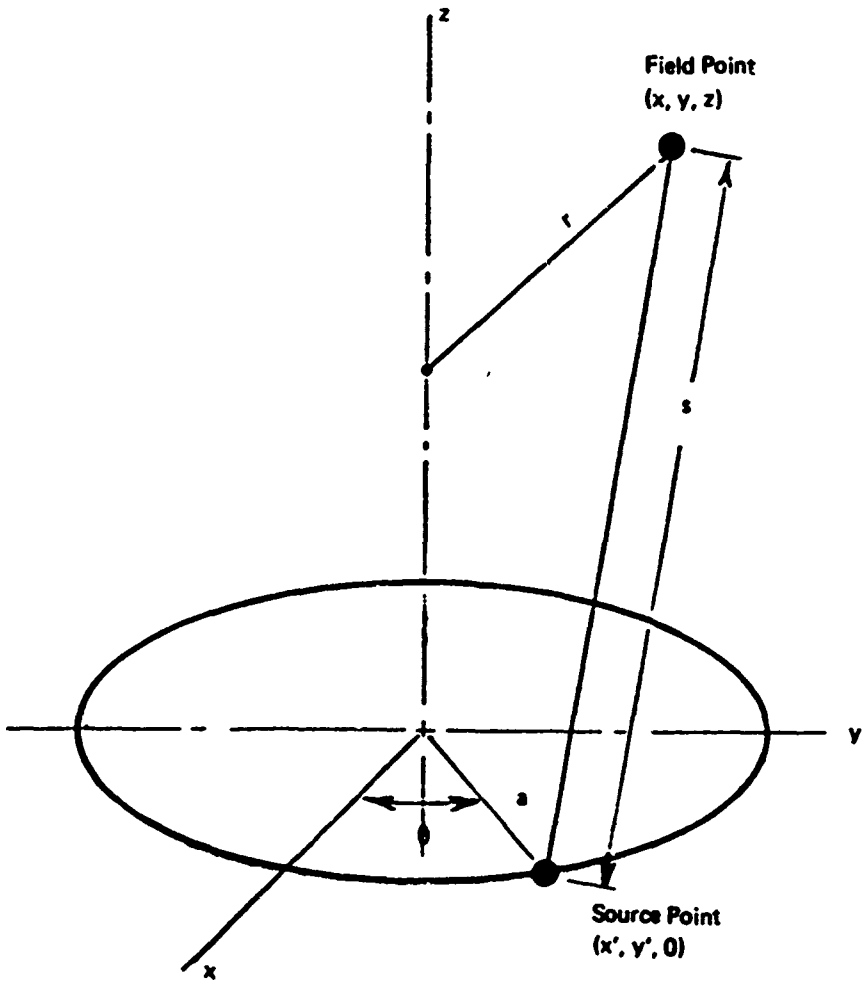

FIGURE C.1 GEOMETRICAL ARRANGEMENT OF THE RING SOURCE & FIELD POINT

APPENDIX D

ANALYSIS OF RADIO FREQUENCY POWER CONTROL

The radio frequency power used to heat the charge will be controlled by a feedback system monitoring the output RF current. Controlling the current controls the RF magnetic field and leaves the conductivity of the charge as the only uncontrolled variable determining the power into the charge. Conductivity increases with increasing temperature. For small penetration depths increased conductivity results in a decrease in input power so that the system is unconditionally stable. For large penetration depths the power input is proportional to conductivity, which varies at most, approximately as the first power of temperature. The power loss from the charge is mostly by radiation and thus varies as the fourth power of the absolute temperature. Therefore, the system will be stable for large skin depth also.

A typical current feedback control system is shown in Figure D.1. The H-Azar recorder is used as a preamplifier, the input summing point, and also to record the error signal. The characteristic time constant of the H-Azar, τ_1, is 0.5 second. The time constants of the RF generator are approximately this same value.

The integral (reset) action, k_c, of the series 80 controller is made as large as possible to obtain accurate steady-state control, while the gains of the H-Azar and the series 80 controller, k_1 and k_b, respectively, and the derivative (rate) action, k_a, of the series 80 controller are adjusted to obtain stable control with minimum response time.

The measured frequency response of a typical control system is shown in Figure D.2. The 1/f slope in the low frequency end of the open look response is due to the integral action of the controller. This system has been adjusted for maximum speed of response, which resulted in the 60° phase margin, the minimum acceptable in good control practice. The resultant closed loop response is good to about 1 Hz.

The last factor in the system dynamics is the thermal transfer function of the charge. We can estimate the thermal time constant, τ_3, by assuming that the heat loss is entirely due to radiation and using the relationship

$$\tau_3 = C_h \frac{dW}{dT}$$

The heat capacity, C_h, = 4.18 Vds (joules/degree) in which V, d and s are the volume, density and specific heat of the charge, respectively. Typical values are

$$V = 40 \text{ cm}^3$$
$$d = 5.5 \text{ gm/cm}^3$$
$$s = 0.1 \text{ cal/gm°K}$$

which result in $C_h = 92$ joule/°K

The heat loss due to radiation is

$$W_r = 5.67 \times 10^{-12} \text{ S } T^4 \quad \text{(watts)}$$

in which S is the radiating surface area

$$dW_r/dT = 22.7 \times 10^{-12} \text{ S } T^3 \quad \text{(watts/degree)}$$

Evaluating this derivative for S = 20 cm^2 (approximately one fourth of the total surface) and T = 3000°K, we obtain dW_r/dT = 12 watts per degree and τ_3 = 8 seconds. Since this is appreciably longer than the response time of the closed loop, temperature fluctuations will be small.

One final consideration is the maximum available power. Power is determined by the magnetic field and, therefore, by the RF current. The current is determined by the inductive reactance of the coil and the output voltage of the RF generator. Since

$$H = \frac{nI}{\ell}, \quad I = \frac{E}{\omega L} \quad \text{and} \quad L \propto n^2$$

decreasing the number of turns, n, in the coil increases the current, I, as n^{-2} and increases the magnetic field, H, and consequently the output power.

Our preliminary coil design calls for a four-turn coil, 1.5 inches long and 1.75 inches mean radius. The coil inductance is given by

$$L = \frac{r^2\, r^2}{10\ell + 9r} = \frac{16 \times 1.75^2}{10 \times 1.5 + 9 \times 1.75} = 1.6 \text{ microhenries}$$

The factor for loss of inductance due to the cross-sectional area of the cage, $\frac{\text{Area coil - Area cage}}{\text{Area coil}}$, is estimated to be about .8, so that the net inductance is about 1.3 microhenries. Assuming that the maximum voltage is 5000 volts and at a frequency of 8 megahertz, we have

$$I = \frac{5000}{2\pi \times 8 \times 10^6 \times 1.3 \times 10^{-6}} = 80 \text{ amperes}$$

and

$$H = \frac{4 \times 80}{1.5\pi \times 2.54 \times 10^{-2}} = 8000 \text{ amperes/meter.}$$

Substituting this value into Equation 17 from Appendix A,

$$W = \frac{2\pi}{15}\, \alpha\, \mu o^2\, w^2\, a^4 c\, Ho^2 \,,$$

with the other parameters

$$\alpha = 50 \text{ mho/meter}$$

$$\mu o = 4\pi \times 10^{-7} \text{ henry/meter}$$

$$w = 5.0 \times 10^7 \text{ radians/second}$$

$$a = .032 \text{ meter}$$

$$c = .01 \text{ meter}$$

we obtain

$$W = 50 \text{ Kilowatts}$$

which is the rated capacity of the RF generator.

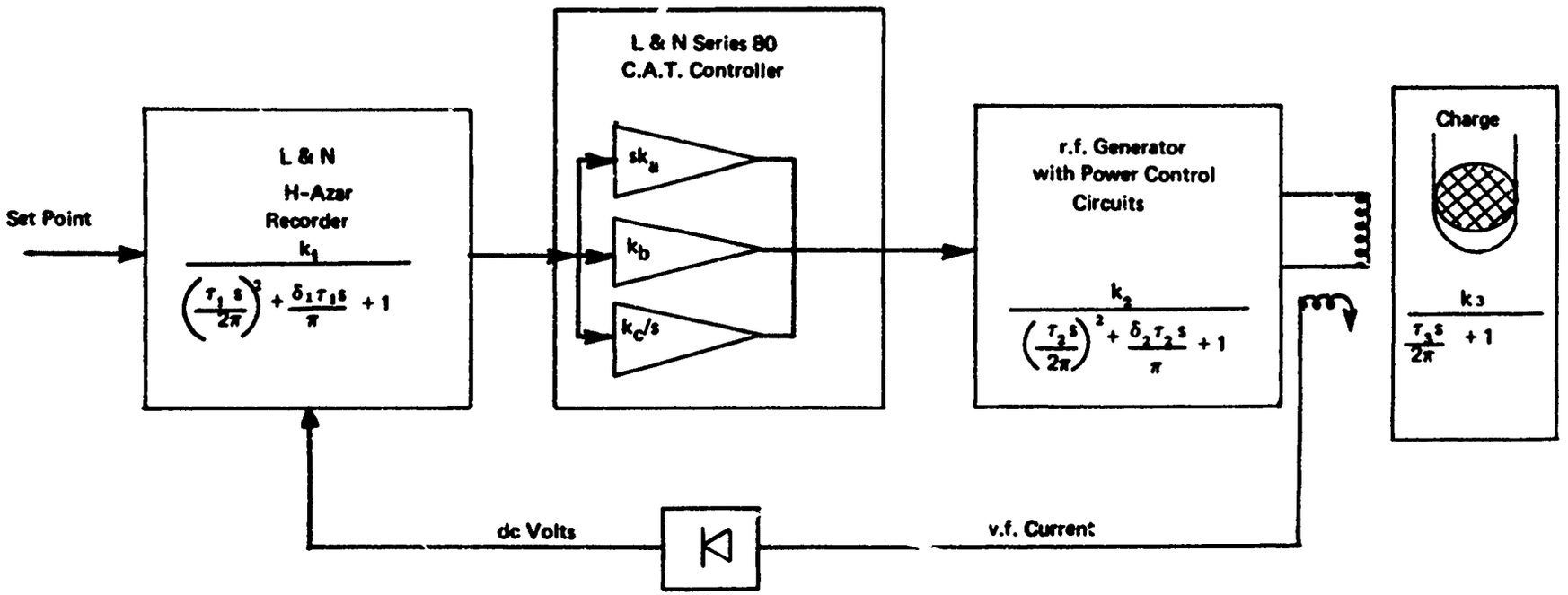

FIGURE D.1 CURRENT FEEDBACK CONTROL SYSTEM

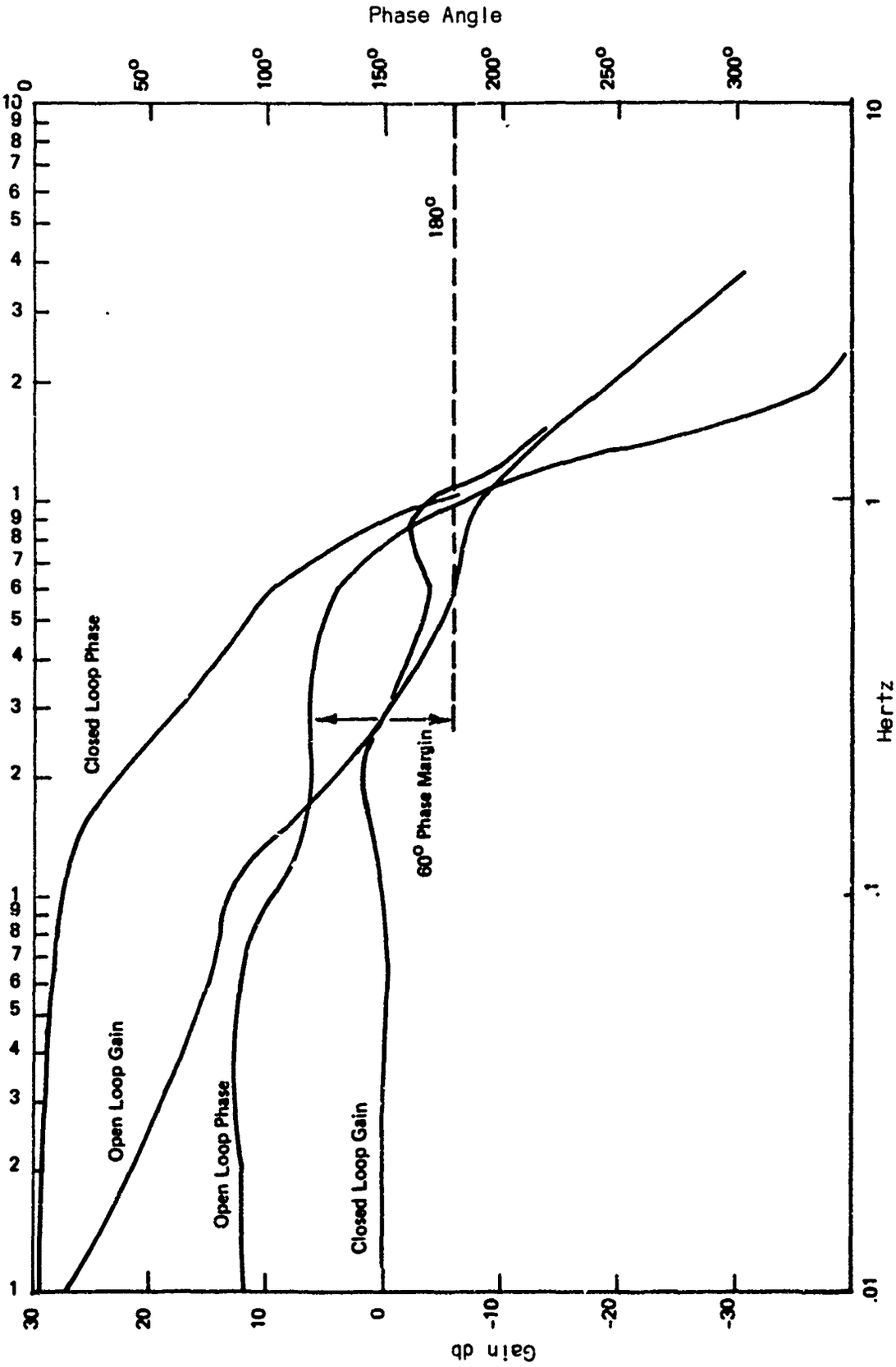

FIGURE D.2 MEASURED FREQUENCY RESPONSE OF A TYPICAL CONTROL SYSTEM